Structural Modification of TiO_2 Nanorod Films with an Influence on the Photovoltaic Efficiency of a Dye-Sensitized Solar Cell (DSSC)

Lijian Meng · Can Li · M. P. dos Santos

Abstract TiO_2 nanorod films have been deposited on ITO substrates by dc reactive magnetron sputtering technique. The structures of these nanorod films were modified by the variation of the oxygen pressure during the sputtering process. Although all these TiO_2 nanorod films deposited at different oxygen pressures show an anatase structure, the orientation of the nanorod films varies with the oxygen pressure. Only a very weak (101) diffraction peak can be observed for the TiO_2 nanorod film prepared at low oxygen pressure. However, as the oxygen pressure is increased, the (220) diffraction peak appears and the intensity of this diffraction peak is increased with the oxygen pressure. The results of the SEM show that these TiO_2 nanorods are perpendicular to the ITO substrate. At low oxygen pressure, these sputtered TiO_2 nanorods stick together and have a dense structure. As the oxygen pressure is increased, these sputtered TiO_2 nanorods get separated gradually and have a porous structure. The optical transmittance of these TiO_2 nanorod films has been measured and then fitted by OJL model. The porosities of the TiO_2 nanorod films have been calculated. The TiO_2 nanorod film prepared at high oxygen pressure shows a high porosity. The dye-sensitized solar cells (DSSCs) have been assembled using these TiO_2 nanorod films prepared at different oxygen pressures as photoelectrode. The optimum performance was achieved for the DSSC using the TiO_2 nanorod film with the highest (220) diffraction peak and the highest porosity.

Keywords TiO_2 · Nanorod · Sputtering · DSSC

1 Introduction

Solar energy, a pollution-free energy source, offers replacement from the traditional energy dependence on fossil fuel and at the same time helps to solve some environmental problems concerning the progress of the our present way of life. It is widely recognized that photovoltaic solar energy conversion has potential to become a major energy source in the near future. Dye-sensitized solar cells (DSSCs) have emerged as the third generation of solar cells because of their potential for low-cost production. Unlike traditional semiconductor solar cells that use wafer substrates, DSSCs are based on the principle of photosynthesis invented by Gratzel in 1991, and use the wide-band gap semiconductor TiO_2 that currently shows over 10 % energy conversion efficiency in laboratory [1, 2]. A DSSC consists of a dye adsorbed on a nanoporous film, typically a TiO_2 film, and an electrolyte used as transport

layer containing redox couples. The dyes on the surface of the films absorb light and inject electrons into the conduction band of the TiO_2. For the electrons to be collected at the transparent conducting layer, an electron should travel the distance in the conduction band from the point where it was injected in the conducting layer, before recombination. The structure of the TiO_2 film will obviously affect the electron transportation and then the solar cell efficiency.

Nanoporous TiO_2 films are generally prepared from a colloidal suspension containing nanosized TiO_2 particles [1–4]. These nanoporous TiO_2 films have huge surface areas and allow a high light collection, maximizing the amount of photogenerated charge. The electron transport is a limiting factor for the performance of these nanoporous TiO_2 films. The porous film must exhibit interconnected particles, to allow the percolation of the injected electrons [5]. The structural disorder at the contact between two nanoparticles enhances the scattering of free electrons, thus reducing the electron mobility [6]. These factors are the limit for further improvements of the conversion efficiency. Therefore, the strongly interconnected and nanoscale ordered photoanode architectures, such as nanotubes [5, 7–9], nanorods [10–12] and nanowires [13, 14], offer the capacity of improvement for electron transport, leading to a higher conversion efficiency. The thicknesses of the TiO_2 films can be reduced dramatically using these ordered nanostructures and they still have a high efficiency, when compared to those using disordered nanostructures.

Most of the nanostructured TiO_2 films were made by chemical methods, which are not easy to reproduce and have some limitations for industrial production. The sputtering technique is a very promising method because it is reproducible and suitable for industry. Although the conversion efficiency still needs to be improved, DSSCs using sputtered TiO_2 films as photoelectrodes have been reported [15–18]. In our previous works, we have prepared TiO_2 nanorod films by dc reactive magnetron sputtering and the effects of the nanorods dimension, blocking layer and annealing temperature on the efficiency of DSSCs have been reported [19–21]. In this study, the TiO_2 nanorod films with different structures have been prepared and the effect of the structures of these nanorod films on the efficiency of DSSCs has been studied.

2 Experimental

The TiO_2 nanorod films were prepared on commercial ITO substrates (with sheet resistance of 20 Ω per square and thickness of 100 nm) by dc reactive magnetron sputtering technique using a commercial sputtering system equipped with a turbo molecular pump. A titanium metal disk (60 mm in diameter and 3 mm in thickness) with a purity of 99.99 % was used as target. After pumping down to 10^{-3} Pa, the oxygen and argon gases (99.99 % purities) were introduced into the chamber through the mass flow controllers. The total sputtering pressure was kept at 1.5 Pa and the oxygen partial pressures were set at 0.09, 0.13, 0.22 and 0.26 Pa, respectively. The target-substrate distance was 50 mm. The deposition time varied from 1 to 3 h in order to get the same thickness for the different oxygen partial pressures. The sputtering was carried out using a constant current. The sputtering current was kept at 0.5 A and the cathode potential was about 440 V with a small oscillation as the oxygen partial pressures was changed. In order to remove the surface contaminants of the target, pre-sputtering was performed for about 20 min with a shutter covering the substrate. The transmittance of the films was measured using a Jasco V-550 UV–Vis spectrophotometer. The XRD measurements have been done using Rigaku miniflex goniometer (30 kV, 15 mA). The morphologies of the nanorods were studied using a field emission scanning electron microscope (FE-SEM). Raman scattering measurements have been performed using a semiconductor laser (and a 532 nm laser line) as exciting light. The laser line was focused on the sample surface in a strict 180° backscattering geometry.

The TiO_2 films were sensitized with N719 dye (Ru(II)L2(NCS)2:2TBA, where L = 2,2′-bipyridyl-4,4′-dicarboxylic acid) by soaking the films in an ethanol solution of N719 dye (0.5 mM) for 24 h at room temperature. The counter-electrode was made by sputtering Pt on an FTO glass and the electrolyte is composed of 0.1 M I_2, 0.1 M LiI, 0.6 M 1-hexyl-3-methylimidazolium iodide, and 0.5 M 4-*tert*-butylpyridine in 3-methoxypropionitrile. The photocurrent–voltage measurements were carried out with a Princeton 2273 Applied Research electrochemical system, and a 500 W Xenon lamp under AM 1.5G illumination and an water filter were used. The light intensity was adjusted to 100 mW/cm^2. Cells with an active area of 0.15 cm^2 were tested.

3 Results and Discussion

The variation of the deposition rate with the oxygen partial pressure is shown in Fig. 1. It can be seen that the deposition rate decreases as the oxygen partial pressure is increased. This happens because of the poisoning (oxidation) of the sputtering target that substantially reduces the sputter erosion rate. During the reactive sputtering process, the composition of the surface of a metal Ti target will depend on the oxygen partial pressure, the target ion current and the sputtering yield of the target material. Some part of the target surface will consist of titanium oxide and

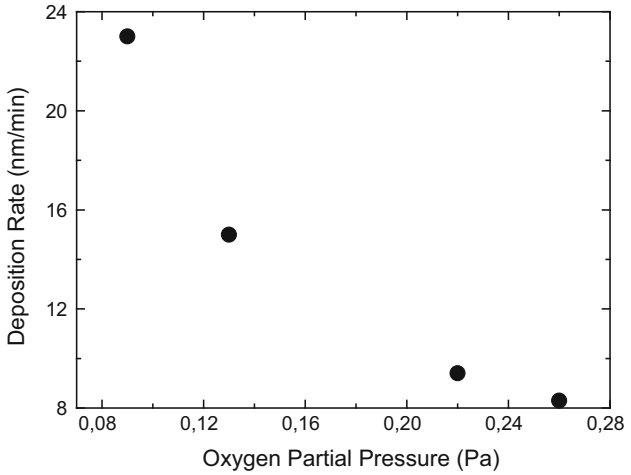

Fig. 1 Deposition rate versus oxygen partial pressure for TiO_2 nanorod films made by dc reactive sputtering

the rest will consist of Ti metal. The relation between these two parts is determined by the competition between the sputtering of titanium oxide from the target and the formation of titanium oxide due to the recombination of the oxygen gas. The titanium oxide formed at the Ti metal target surface has a lower sputtering yield than the pure Ti metal, causing a lower deposition rate. As the oxygen partial pressure is increased, the area covered by titanium oxide at the Ti metal target surface increases and results in a drop of the deposition rate.

Figure 2 shows the FE-SEM images for TiO_2 nanorod films made at different oxygen partial pressures. Based on these SEM images, it can be seen that the nanorods are all aligned in the same direction, perpendicular to the substrate surface. At low oxygen partial pressure, the TiO_2 nanorods stick together and have a dense structure. As the oxygen partial pressure is increased, these sputtered TiO_2 nanorods become gradually more separated and present a porous structure. It can also be seen from the SEM images that the length of the nanorods is about 1,000 nm. These nanorods are not uniform. The dimension varies from tens of nm to hundreds of nm. The longer nanorods are composed of nanorods with smaller dimensions and then they will separate further into nanorods with smaller dimensions by decreasing the energy of the sputtered particles [19]. X-ray diffraction patterns taken from TiO_2 nanorod films prepared on ITO substrates at different oxygen partial pressures are shown in Fig. 3, along with the pattern of the ITO substrate, for comparison. It can be seen that all samples consist entirely of anatase phase, and no other phase has been observed. For the sample prepared at 0.09 Pa oxygen partial pressure, only a weak diffraction peak along the (101) direction has been observed. As the oxygen partial pressure is increased, another diffraction peak appears along the (220) direction. The intensity of the (101) peak does not show a clear variation with the oxygen partial pressure, but the intensity of the (220) peak increases with the oxygen partial pressure. It means the TiO_2 nanorods prepared at high oxygen partial pressure show a very strong preferred orientation along the (220) direction. Based on these results, although all the TiO_2 nanorods prepared at different oxygen partial pressures have only anatase phase,

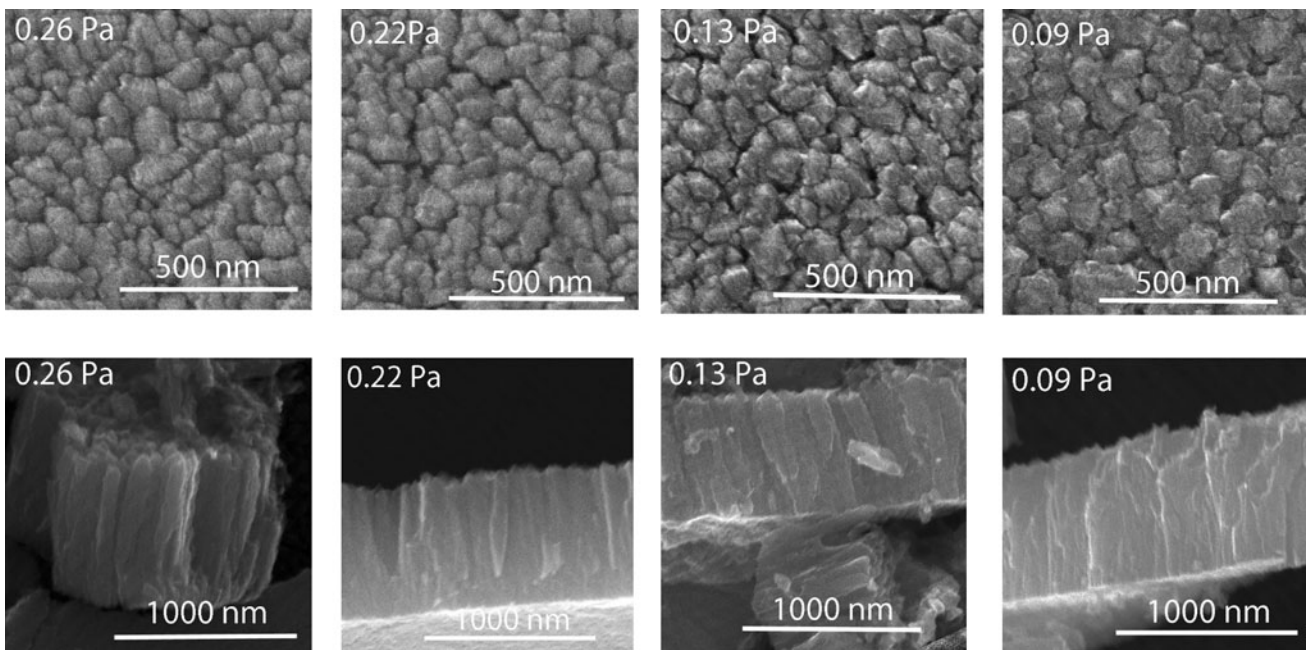

Fig. 2 FE-SEM images for TiO_2 nanorod films made by dc reactive sputtering at different oxygen partial pressures

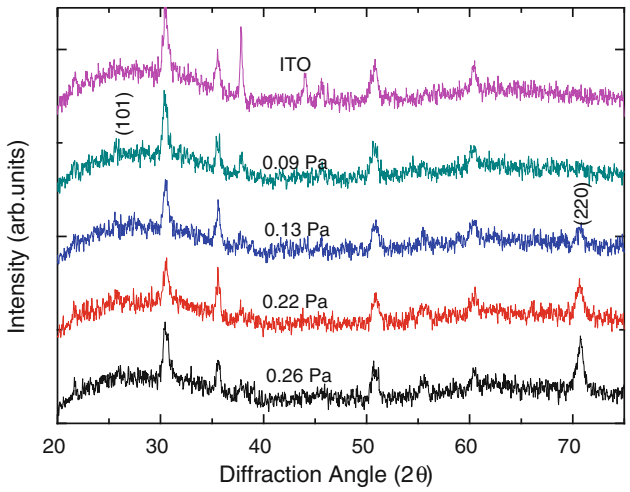

Fig. 3 X-ray diffraction patterns taken from TiO_2 nanorod films made by dc reactive sputtering at different oxygen partial pressures

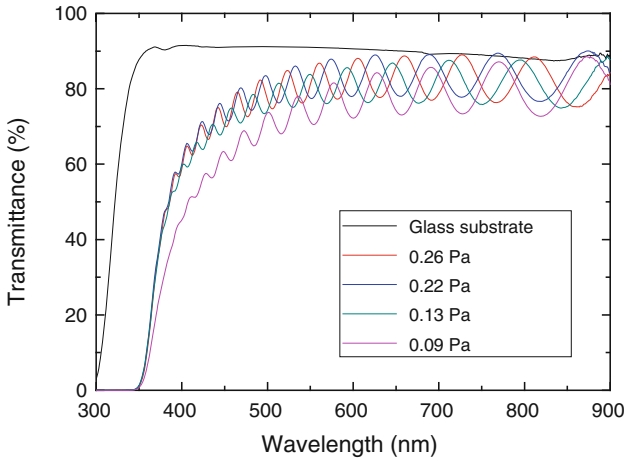

Fig. 4 Specular transmittance spectra of TiO_2 nanorod films made by dc reactive sputtering at different oxygen partial pressures

the growth direction can be modified by changing the oxygen partial pressure.

The specular transmittance spectra of TiO_2 nanorod films prepared at different oxygen partial pressures are shown in Fig. 4. For comparison, the transmittance of the glass substrate is also shown in the figure. It can be observed that the transmittance increases as the oxygen partial pressure is increased from 0.09 to 0.22 Pa. When the oxygen partial pressure is higher than 0.22 Pa, the transmittance does not present a significant variation. The TiO_2 nanorods prepared at low oxygen partial pressure have not a good stoichiometric ratio, many oxygen vacancies exist and this results in a low transmittance. As the oxygen partial pressure is increased, TiO_2 nanorods can be obtained with a good stoichiometric ratio. Therefore, the formation of oxygen vacancies strongly decreases, causing

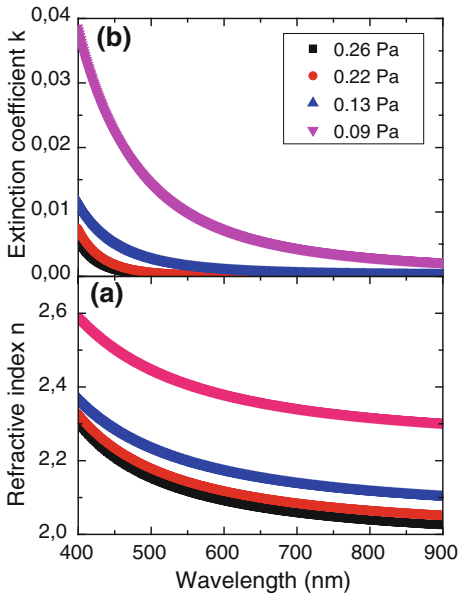

Fig. 5 Refractive index (**a**) and extinction coefficient (**b**) versus wavelength for TiO_2 nanorod films made by dc reactive sputtering at different oxygen partial pressures

an increase of the transmittance. In order to get the porosity of these nanorods, the transmittance has been fitted by the interband transition of the O'Leary-Johnson-Lim (OJL) model [22] and the refractive index **n** and the extinction coefficient **k** have been obtained from the fitting, as shown in Fig. 5. It can be seen clearly that the refractive index of these TiO_2 nanorods decreases as the oxygen partial pressure is increased. It indicates that the porosity of these TiO_2 nanorods increases as the oxygen partial pressure is increased. This fact has been confirmed by SEM measurements. These measurements show the separated TiO_2 nanorods that will cause a higher porosity as the oxygen partial pressure is increased. The porosity of these TiO_2 nanorods has been estimated using the equation [23]:

$$n_f = n_s(1 - q) + n_v q \quad (1)$$

where **q** is the porosity, $\mathbf{n_v}$ is the refractive index of the TiO_2 void filling material and $\mathbf{n_s}$ is the refractive index of bulk TiO_2 material. If we assume that all the voids are filled with air, then $n_v = 1$. For anatase TiO_2 bulk material, $n_s = 2.57$. Using these data and $\mathbf{n_f}$ at 500 nm, the porosities the TiO_2 nanorods have been calculated and they are given in Table 1. It can be seen that the porosity of these TiO_2 nanorods has an important increase from 8 to 22 % as the oxygen partial pressure is increased from 0.09 to 0.13 Pa. When the oxygen partial pressure is increased from 0.13 to 0.26 Pa, the porosity shows a small variation from 22 to 27 %. These variations may be related to the modification of the structure of these nanorods. As XRD patterns show, when the oxygen partial pressure is 0.09 Pa,

Table 1 Cell performance

Sample	Oxygen pressure (Pa)	J_{sc} (mA/cm^2)	V_{oc} (V)	FF	η (%)	Porosity (%)
1	0.09	1.32	0.54	0.59	0.42	8
2	0.13	2.35	0.62	0.69	1.01	22
3	0.22	2.86	0.64	0.72	1.32	25
4	0.26	3.32	0.64	0.65	1.38	27

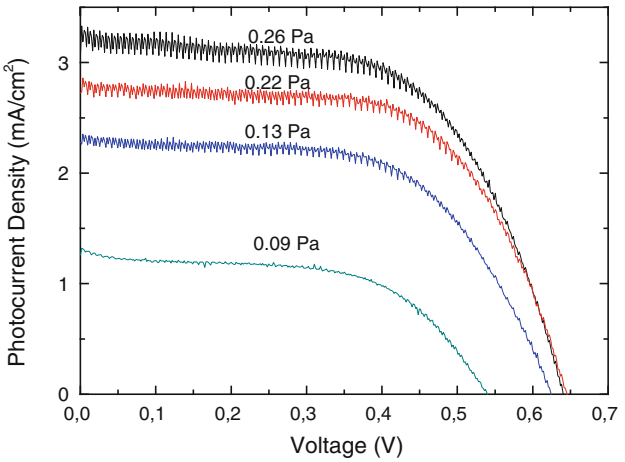

Fig. 6 Photocurrent–voltage plots of DSSC assembled with TiO_2 nanorod films made by dc reactive sputtering at different oxygen partial pressures

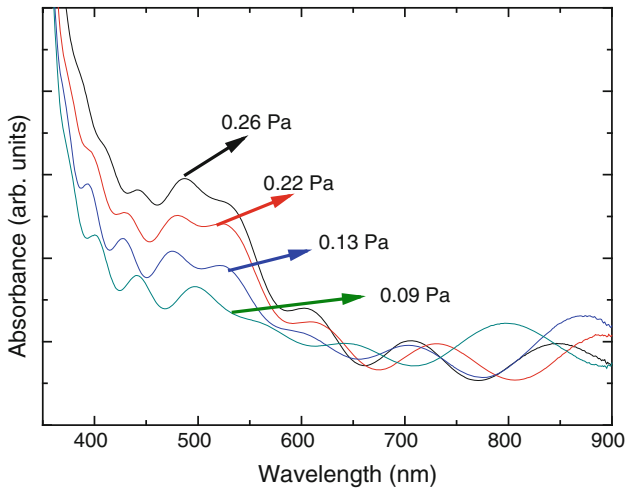

Fig. 7 UV–Vis spectra of TiO_2 nanorod films made by dc reactive sputtering at different oxygen partial pressures after dye-sensitized

the TiO_2 nanorods present an orientation along the (101) direction; when the oxygen partial pressure is higher than 0.13 Pa, the TiO_2 nanorods present an orientation along the (220) direction. The TiO_2 nanorods with a preferred growth along the (101) direction have a lower porosity than those growing along the (220) direction.

The photocurrent–voltage plots of DSSCs assembled with TiO_2 nanorod films prepared at different oxygen partial pressures are given in Fig. 6. The cell performance parameters, such as the short-circuit current $\mathbf{J_{sc}}$, the open circuit voltage $\mathbf{V_{oc}}$, the fill factor **FF** and the conversion efficiency **η**, have been listed in Table 1. It can be seen that both $\mathbf{J_{sc}}$ and $\mathbf{V_{oc}}$ exhibit an important increase when the oxygen partial pressure is raised from 0.09 to 0.13 Pa. The DSSCs assembled using TiO_2 nanorods prepared at high oxygen partial pressure show higher photocurrent and higher conversion efficiency. The two main factors influencing the photocurrent are the dye adsorption and the electron transportation. The dye adsorption has been qualitatively characterized by measuring the absorbance in the visible region as shown in Fig. 7. The absorption around the 500 nm in Fig. 7 comes from the dye N719. The variation of the absorbance of the dye roughly agrees with the variation of the photocurrent: the more absorbance it has, a higher photocurrent is obtained. However, attention should be paid to the samples prepared at 0.09 and

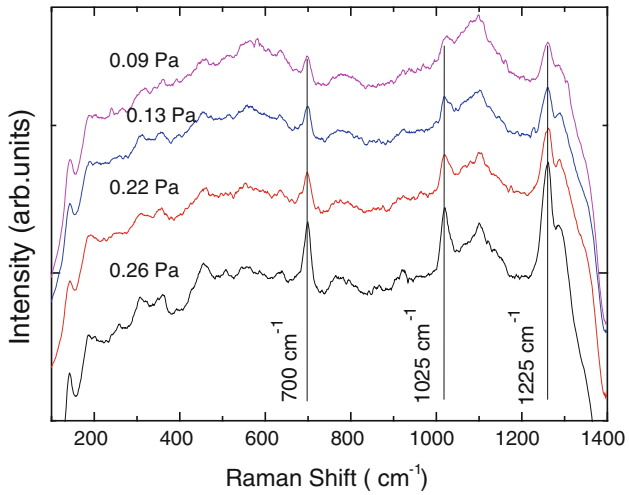

Fig. 8 Raman spectra of TiO_2 nanorod films made by dc reactive sputtering at different oxygen partial pressures after dye-sensitized

0.13 Pa. From Fig. 6 it can be seen that when the oxygen partial pressure is increased from 0.09 to 0.13 Pa, the photocurrent shows an important increase. But from Fig. 7 it can also be seen that the dye absorbance does not show a significant variation compared to the other samples. This means that this big increase of the photocurrent is not originated from the dye adsorption, it comes from the

improvement of the electron transportation. The TiO_2 nanorods change their orientation from the (101) to the (220) directions when the oxygen partial pressure is increased from 0.09 to 0.13 Pa, as shown in Fig. 3. This suggests that the (220) oriented TiO_2 nanorods are more adequate for DSSC applications, because the (220) orientation seems to be more favorable for electron transportation and results in a higher photocurrent. The dye adsorption can be also characterized qualitatively by the Raman spectra. Figure 8 shows the Raman spectra of TiO_2 nanorod films prepared at different oxygen partial pressures after dye-sensitization. The three Raman peaks located at 700, 1,025 and 1,225 cm^{-1} are those from the N719 dye. From this figure it can be seen that N719 Raman peaks intensity increases as the dye adsorption is increased. This is another way to characterize the dye absorbance. The maximum conversion efficiency (1.38 %) is obtained for TiO_2 nanorods prepared at the oxygen partial pressure of 0.26 Pa. Although this is not high conversion efficiency, it shows another technique for DSSC, which is more suitable for industrial production. Furthermore, considering the length of these nanorods (only about 1,000 nm), the efficiency can be improved by increasing the length of the nanorods. The efficiency of 5 % has been achieved for the length of 3,000 nm of the TiO_2 nanorods [24].

4 Conclusions

TiO_2 nanorods have been prepared both on ITO and glass substrates by dc reactive magnetron sputtering. Changing the oxygen partial pressure during the preparation processes can modify the structure of these nanorods. The TiO_2 nanorods prepared at oxygen partial pressures lower than 0.09 Pa show an orientation along the (101) direction and those prepared at the oxygen partial pressures higher than 0.09 Pa show an orientation along the (220) direction. The DSSCs have been assembled using these TiO_2 nanorods. The nanorods with the (220) orientation are favorable for the electron transportation, resulting in a high photocurrent and then a high conversion efficiency. The Raman scattering spectroscopy can be used to qualitatively characterize the dye adsorption. The intensity of N719 Raman peaks, located at 700, 1,025 and 1,225 cm^{-1}, increases as the dye adsorption is increased.

References

1. B. Oregan, M. Gratzel, Nature **353**(6346), 737 (1991)
2. Y. Chiba, A. Islam, R. Komiya, N. Koide, L.Y. Han, Appl. Phys. Lett. **88**(22), 223505 (2006)
3. S.J. Yuan, Y.G. Li, Q.H. Zhang, H.Z. Wang, Electrochim. Acta **79**, 182 (2012)
4. A.H. Ramelan, H. Harjana, L.S. Sakti, Proc. Spie **8435**, 84352F (2012)
5. C. Longo, M.A. De Paoli, J. Brazil. Chem. Soc. **14**(6), 889 (2003)
6. G.K. Mor, K. Shankar, M. Paulose, O.K. Varghese, C.A. Grimes, Nano Lett. **6**(2), 215 (2006)
7. Y. Ohsaki, N. Masaki, T. Kitamura, Y. Wada, T. Okamoto, T. Sekino, K. Niihara, S. Yanagida, Phys. Chem. Chem. Phys. **7**(24), 4157 (2005)
8. S. Ngamsinlapasathian, S. Sakulkhaemaruethai, S. Pavasupree, A. Kitiyanan, T. Sreethawong, Y. Suzuki, S. Yoshikawa, J. Photochem. Photobiol. a-Chem. **164**(1–3), 145 (2004)
9. P. Zhong, W.X. Que, Y.L. Liao, J. Zhang, X. Hu, J. Alloy Compd. **540**, 159 (2012)
10. B.H. Lee, M.Y. Song, S.Y. Jang, S.M. Jo, S.Y. Kwak, D.Y. Kim, J. Phys. Chem. C **113**(51), 21453 (2009)
11. S.H. Kang, S.H. Choi, M.S. Kang, J.Y. Kim, H.S. Kim, T. Hyeon, Y.E. Sung, Adv. Mater. **20**(1), 54 (2008)
12. F. Xu, Y. Wu, X.Y. Zhang, Z.Y. Gao, K. Jiang, Micro Nano Lett. **7**(8), 826 (2012)
13. M. Law, L.E. Greene, J.C. Johnson, R. Saykally, P.D. Yang, Nat. Mater. **4**(6), 455 (2005)
14. X.J. Feng, K. Shankar, O.K. Varghese, M. Paulose, T.J. Latempa, C.A. Grimes, Nano Lett. **8**(11), 3781 (2008)
15. M. Gomez, E. Magnusson, E. Olsson, A. Hagfeldt, S.E. Lindquist, C.G. Granqvist, Sol. Energy Mater. Sol. Cells **62**(3), 259 (2000)
16. Y.M. Sung, H.J. Kim, Thin Solid Films **515**(12), 4996 (2007)
17. S.H. Kang, M.S. Kang, H.S. Kim, J.Y. Kim, Y.H. Chung, W.H. Smyri, Y.E. Sung, J. Power Sources **184**(1), 331 (2008)
18. S.H. Kang, J.W. Lim, H.S. Kim, J.Y. Kim, Y.H. Chung, Y.E. Sung, Chem. Mater. **21**(13), 2777 (2009)
19. L.J. Meng, T. Ren, C. Li, Appl. Surf. Sci. **256**(11), 3676 (2010)
20. L.J. Meng, C. Li, Nanosci. Nanotechnol. Lett. **3**(2), 181 (2011)
21. L.J. Meng, C. Li, M.P. dos Santos, J. Inorg. Organomet. Polym. **21**(4), 770 (2011)
22. S.K. O'Leary, S.R. Johnson, J. Lim, J. Appl. Phys. **82**(7), 3334 (1997)
23. Y. Tachibana, H.Y. Akiyama, S. Kuwabata, Sol. Energy Mater. Sol. Cells **91**(2-3), 201 (2007)
24. L.J. Meng, A.F. Ma, P.L. Ying, Z.C. Feng, C. Li, J. Nanosci. Nanotechnol. **11**(2), 929 (2011)